Sensor Fusion for Force and Position Calibration of a Motorized Surgical Smart Grasper

1st Jack Kaplan
dept. Mechanical Engineering
University of Washington
Seattle, WA, USA
jack.m.kaplan@gmail.com

2nd Yana Sosnovskaya
dept. Electrical and Computer Engineering
University of Washington
Seattle, WA, USA
ysos@uw.edu

3rd Matthew Arnold
dept. Computer Science and Engineering
University of Washington
Seattle, WA, USA
mma35@uw.edu

4th Blake Hannaford
dept. Electrical and Computer Engineering
University of Washington
Seattle, WA, USA
blake@uw.edu

Abstract—**Minimally Invasive Surgery lacks tactile feedback that surgeons find useful for finding and diagnosing tissue abnormalities. The goal of this paper is to calibrate sensors of a motorized Smart Grasper surgical instrument to provide accurate force and position measurements. These values serve two functions with the novel calibration hardware. The first is to control the motor of the Grasper to prevent tissue damage. The second is to act as the base upon which future work in multi-modal sensor fusion tissue characterization can be built. Our results show that the Grasper jaw distance is a function of both applied force and motor angle while the force the jaws apply to the tissue can be measured using the internal load cell. All code and data sets used to generate this paper can be found on GitHub at https://github.com/Yana-Sosnovskaya/Smart_Grasper_public**

Index Terms—**Surgical Robotics, force sensing, sensor fusion**

I. INTRODUCTION

Minimally Invasive Surgery (MIS) has become standard in modern medicine and involves operating through small incisions using laparoscopic instruments (graspers) for manipulation and endoscopic cameras for visual feedback. Advantages of MIS include faster recovery, less blood loss, and a lower risk of complications.

Alongside its benefits, MIS also brings new challenges, such as a lack of tactile feedback for surgeons [1], [2]. In open surgery, surgeons can palpate the tissue to gain information about non-visible structures such as the location of tumors and blood vessels [1], [3]. Moreover, force sensing is crucial for avoiding tissue trauma during grasping in abdominal surgeries. Excessive forces will cause tissue to be traumatized, and insufficient forces can lead to instrument slippage reducing operation efficiency and endangering

patient safety [4], [5]. Conventional laparoscopic surgical instruments still lack force sensing, making diagnostic quality tactile feedback infeasible [2]–[4].

Multiple laparoscopic graspers with force sensors have been designed to provide the force measurements necessary for useful tactile feedback. One example is the laparoscopic grasping tool developed by [6] for the Raven-II surgical robot [7]. This tool has the capability of sensing a three-axis Cartesian manipulation force and a single-axis grasping force, using two torque sensors embedded in driving pulleys of the Raven-II surgical robot. Kim *et al.* [8], [9] take another approach that uses capacitive transducers with an analog signal processing unit embedded in the instrument's tip.

A multi-modal approach was used in building sensorized-forceps by [10]. Their work mostly focused on compensating for environmental influences (e.g. temperature and humidity change) that affect force measurements. Other surgical instruments use strain gauges for direct [11] and indirect [12] force measurement. Soakhanvar *et al.* [13] used three uniaxial polyvinylidene fluoride (PVDF) films based on the piezoelectric effect to measure force, the location of concentrated load (e.g. a hidden lump) and the softness of the grasped object. Recent research developed by [14] presents a novel clamping force sensor based on fiber Bragg grating integrated in a manual laparoscopic instrument and tested on both *ex-vivo* tissue and *in-vivo* porcine liver.

The existing work in this field is vast, but no instrument is ready for the operating room. Some of them have a good measurement range and sensitivity but are too big to use on actual surgical instruments [15]; MIS port sizes are typically between 5 and 10 mm in diameter [16]. Others lack measurement range [6], are insufficiently sensitive [2], or are unlikely to survive sterilization [17]. Additionally, many of these surgical instruments only close in set increments rather
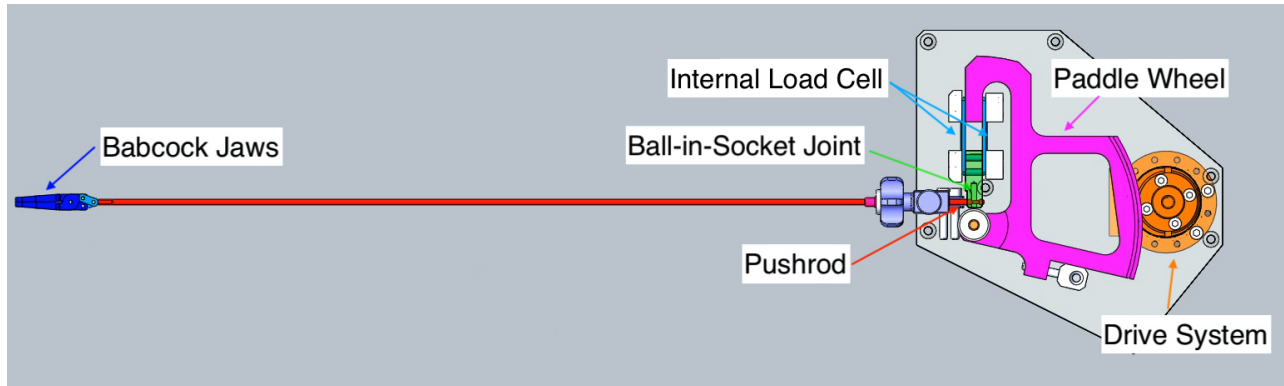
Fig. 1: The Smart Grasper (formerly MEG) without its top cover. The drive system turns a paddle wheel using a steel rope (not shown). The paddle wheel is attached to a ball-in-socket joint that moves the pushrod back and forth, which opens and closes the Babcock jaws. Readings from the internal load cell record the force on the pushrod.

than having a continuous range of motion. This lack of fine position control could lead to tissue deformation and damage if the force needed to close a given amount is above the safe threshold for a particular tissue [4], [5].

In this paper, we address these issues by building on the Motorized Endoscopic Grasper (MEG), first developed by [18]. The MEG employs force and position sensors to provide continuous, one-dimensional jaw position and force measurements while grasping tissue. To differentiate the planned multi-modal tissue classification setup from previous work, we rename the MEG to the *Smart Grasper*.

A new calibration setup was built in order to verify and improve upon the calibration procedures previously developed by Roan *et al.* [19], [20]. The accuracy of the other modalities (e.g. pulse oximetry, bioimpedance, temperature, ultrasound) that will be placed on the jaws of the Smart Grasper is dependent on the quality of the force and position calibration. Accurate force calibration will also allow for a controller that reduces damage to tissue resulting from excessive applied force.

II. METHODS

A. Hardware

The mechanical hardware was mostly unchanged from [18]. Fig. 1 demonstrates how the motor (RE25-10 W, Maxon) with attached 19:1 planetary gearbox (GP26, Maxon) and encoder (HEDL55, Maxon) opened and closed the Grasper tip's jaws.

While the Grasper's mechanical hardware remained untouched, a few changes were made to the sensing and controls. An updated motor controller (2018 ESCON 50/5 4-Q Servocontroller, Maxon) is controlled via microcontroller (Teensy 4.0) by Pulse-Width Modulation (PWM) in current control mode. The relationship between the PWM input and the command current was linear but varied based on controller setup parameters. For all the data gathered in this paper, the motor controller was set to output anywhere from $0-400$ mA of current. A quadrature encoder buffer breakout board (LS7366R, SuperDroid Robots) keeps track of encoder counts at 40 MHz.

Only one of the internal force sensors (FR1010, 40 lb, FUTEK) was used because of damage to the second's wiring during storage, but no need could be found to have two load cells besides redundancy. After amplification (CSG110, FUTEK), a 10 bit analog-to-digital converter (ADC) maps the $0-5$ V force sensor output to discretized values (DV) ranging from $0-1023$.

The test fixture consisted of a wooden base with screw points to attach the Grasper and the smaller calibration subassemblies (sections II-B1 and II-C1).

B. Force Calibration

1) Subassembly Design: The force calibration fixture (Fig. 2) was attached to the mount described in section II-A and consisted of an aluminum plate connected to the external load cell (TAL220B, 5 kg). The upper Grasper jaw engaged with the plate and the lowered jaw engaged with a 3D printed base, as seen in Fig. 2. Raising the external load cell and lowering the 3D printed piece increased the jaw distance. Output from the external load cell was routed through a breakout board (HX711, Sparkfun) with an amplifier and a 24 bit ADC before going to the microcontroller.

2) External Load Cell Calibration: Determining the relationship between the external load cell DV and forces measured in newtons required applying known forces to the load cell and recording the measurement. We hung masses from a 3D printed fixture as shown in Fig. 3.

Fig. 4 shows both the data collected as well as the best fit line relating the external load cell DV to newtons. The coefficient values for (1) were found using a least squares regression.

$$F(z) = c_0 + c_1 z \tag{1}$$

where z is the force reading from the external load cell measured in DV and F is the force measurement in newtons. This line has a root mean square error (RMSE) of 0.0879 N and an R^2 value of 1.00. Looking at Fig. 4 further illustrates the goodness of the fit and suggests that the RSME would be even lower if not for one outlying data point. Values for c_0 and c_1 can be found in Table I.
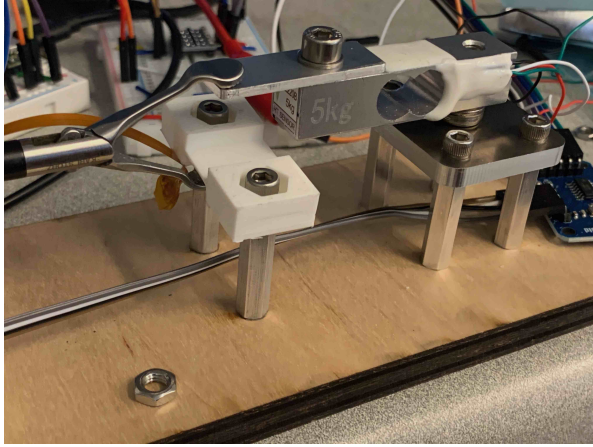
Fig. 2: Force Calibration Fixture with external load cell. HX711 breakout board not shown. The external load cell and the 3D printed piece were raised and lowered by adding and removing washers.
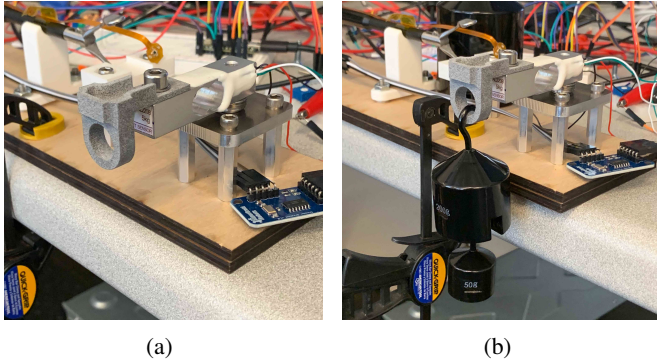

(a)

(b)

Fig. 3: Unloaded (a) and loaded (b) fixture for calibrating external load cell readings to known forces.

The $0 - 16$ N range of data gathered spans the operable space. The Grasper jaws have an area of 56.4 mm^2, so applying 16 N would produce just under 284 kPa of pressure. This much pressure is above the $160 - 280$ kPa range that caused liver failure with the Smart Grasper in [5].

3) Internal Load Cell Calibration: Grasper and external load cell data were recorded from forces created by the drive
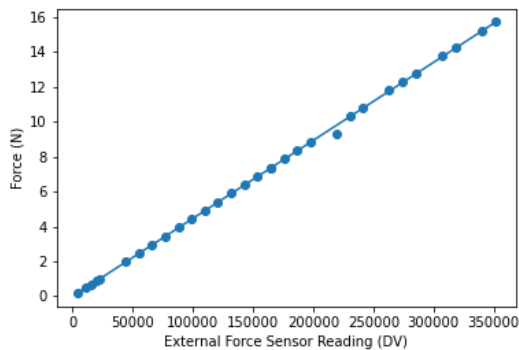

Fig. 4: A curve mapping the external load cell readings to newtons. The curve has an RSME of 0.0879 N and an R^2 of 1.00.

TABLE I: External Load Cell to Newtons Coefficient Values

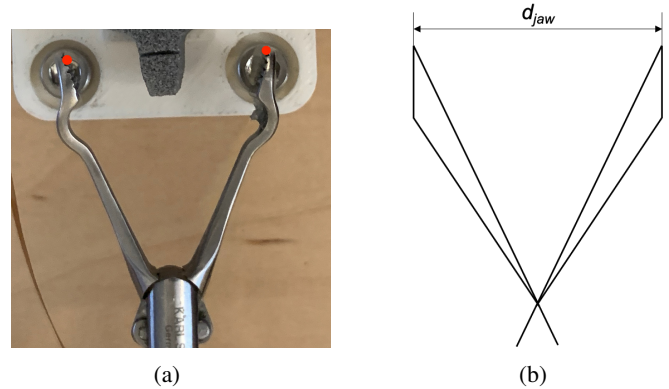| Coefficient	Value	Units
c_0	-5.63×10^{-3}	N
c_1	4.46×10^{-5}	N per external DV

(a)

(b)

Fig. 5: Jaw Distance. Note that the distance between the red dots in (a) corresponds to d_{jaw} in (b).

motor and pushrod. The Grasper was fed an incrementally increasing current and the average load cell readings for each were recorded. Encoder data was recorded as well because [19] claimed that jaw distance also impacted the measured force. For the same reason, the calibration process was repeated for different jaw distances.

C. Position Calibration

Being able to accurately determine the distance between the Grasper's jaws is crucial to combining data from other planned sensor modalities into a cohesive picture of the tissue being grasped.

In an infinitely stiff grasper, there would be an direct relationship between the motor rotation to jaw distance. However, stretching and bending of the mechanical components add compliance between the motor angle (measured by an encoder) and the jaw distance (d_{jaw} in Fig. 5). Therefore, the jaw distance is a function of both motor angle and applied force (see (6)). Deformation and slack in the system will vary with force and the state of the cable.

1) Subassembly Design: The position calibration fixture is a block of known width upon which the Grasper jaws squeeze (Fig. 6). These blocks were 3D printed and range in size from 5 mm to 19 mm in 1 mm increments.

2) Procedure: The position calibration procedure began by putting a block with known width in the fixture (Fig 7). The Grasper was then fed a current causing it grasp the block (Fig. 6). Calipers were used to measure the actual distance between the jaws to the nearest 0.1 mm. The current to the Grasper was increased, and measurements from the internal force sensor and the motor encoder during this process were recorded. The process was then repeated for every block.

Each run of the calibration process can record data for multiple distances. The encoder was zeroed by feeding a Grasper a current that causes the jaws to open until they reach a mechanical stop. The point at which the jaws cannot
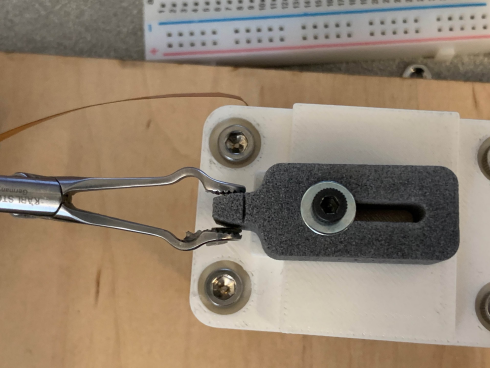
Fig. 6: Grasper jaws squeeze a 5 mm block during the position calibration process. During setup, the block is placed so that the measured jaw distance is collinear with the measurement line across the tip.

Fig. 7: Position calibration subassembly with 5 mm block.

open any wider is made the zero point. This was done at the start of each run and every time a new block was put into the position fixture. Zeroing the encoder every time a new block was put into the position fixture prevented error accumulating when manually aligning the jaws to the measurement line. The error that zeroing the encoder addressed only occurred during the manual manipulation of the Grasper and so should not be an issue during normal use.

III. RESULTS AND DISCUSSION

The Python 3.8 function `scipy.opimize.curve_fit` was used for all surface fitting. Both quadratic and linear surface fits were tried for the position and the force fit.

The purpose of this regression analysis is to find a calibration function that takes the sensor readings as inputs and outputs a value close enough to the true value to be usable. Both overfitting and underfitting optimization curves can reduce their predictive power. Given the relatively small size of the data sets, the risk of overfitting is greater than the risk of underfitting. Therefore, even though the quadratic better fit the current data, the linear fit was chosen. The improvement was not enough to justify the increased risk of overfitting.

A. Force Calibration

1) Force Surface Fit: The best fit planar surface for the force calibration is defined by:

$$z(x, y) = c_2 + c_3 x + c_4 y \qquad (2)$$

where x is the internal force sensor reading in DV, y is the encoder reading in counts, and z is the same as in (1). Values for c_2, c_3, and c_4 were not found for this step. Instead, a direct relationship between the internal load cell and the force at the Grasper's tip measured in newtons was found by substituting (2) into (1). This action yields:

$$F(x, y) = c_0 + c_1 (c_2 + c_3 x + c_4 y) \qquad (3)$$

which can be simplified to:

$$F(x, y) = \alpha + \beta x + \gamma y \qquad (4)$$

The values for α, β, and γ can be found in Table II and the resulting surface can be seen in Fig. 8. This fit has an RMSE of 0.980 N and a mean absolute error (MAE) of 0.721 N. Given the quality of the fit found in section II-B2, (1) was treated as true for the purpose of determining the error of the final planar fit.

TABLE II: Grasper Force Reading to Jaw Tip Force Coefficient Values

Coefficient	Value	Units
α	-0.484	N
β	1.70×10^{-2}	N per Grasper DV
γ	-1.54×10^{-5}	N per encoder count

The error between the measured and calculated force values exerted by the Grasper's jaws appears to be normally distributed around zero (the actual calculated mean error is -5.11×10^{-9} N) with a standard deviation of 0.980 N.

2) Curve Fit: The small value for γ in (4) indicates that the encoder value plays little role in determining the force applied at the Grasper tip. Another way to demonstrate the encoder's negligible impact is by determining the quality of the fit without the encoder. A 1D linear regression mapping the internal force sensor to the measured force at the jaws (Fig. 9) has an RSME of 0.989 N, barely more than the RSME from the surface fit. This curve fit is defined by

$$F(x) = \zeta + \phi x \qquad (5)$$

with F is the jaw force measurement in newtons and x is the internal force sensor measured in DV. The values of ζ and ϕ can be found in Table III.
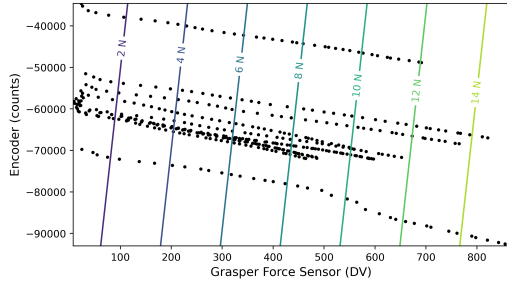
TABLE III: Force Measurement Linear Regression Coefficient Values

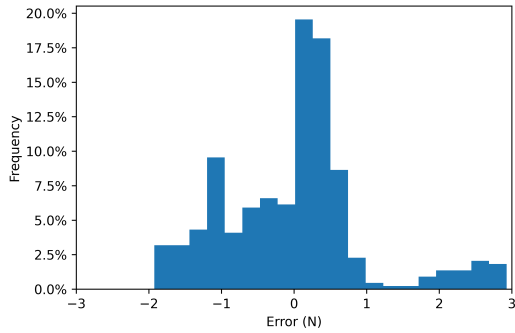| Coefficient	Value	Units
ζ	0.0402	N
ϕ	1.73×10^{-2}	N per Grasper DV

The error of this curve fit appears to be normally distributed with a mean of zero (the calculated mean error is 1.22×10^{-15} N) and a standard deviation of 0.989 N.
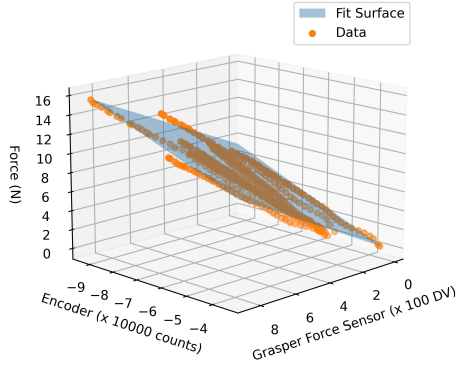
(a) Force surface fit plot


(b) Force fit contour plot
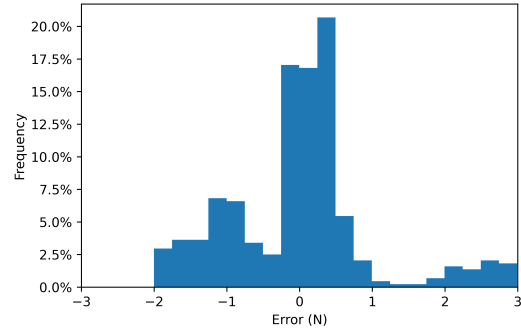

(c) Force fit error distribution

Fig. 8: Planar surface fit for force calibration. The best fit surface is plotted alongside (a) the measured data in 3D and (b) a 2D contour plot. The distribution of the error between the measured and calculated force for a given force-encoder pair is shown in (c).

3) Comparison to Previous Work: Roan *et al.* [19] use the linkage geometry to get a set of equations relating the force measured by the internal load cell to the force at the jaw tip. These equations do indeed depend on the jaw angle θ which is directly related to the jaw distance d_{jaw}. However, these equations do not account for disturbances in the system such as backlash, friction, and deformation. Roan *et al.* add an "adjusted jaw displacement factor" to better fit their equations to the data, but they attribute this fudge factor only to "measurement errors in link length" [19, pp. 182-183].

Rather than try to model all possible deviations from the perfectly rigid, frictionless environment assumed in [19], we
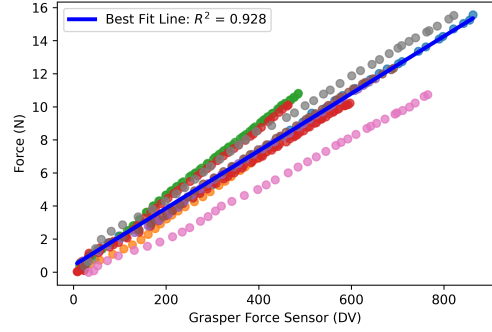
(a) Force curve fit plot

(b) Force curve fit error distribution

Fig. 9: 1D linear curve fit for force calibration. (a) The best fit line is plotted alongside the measured data. Different colored data points are from different trials. The distribution of the error between the measured and calculated force for a given Grasper force reading is shown in (b). The R^2 value of this fit is 0.928.

used the data generated in section II-B to determine the relationship between the applied force and the measured force. Our standard deviation of 0.99 N is worse than the 0.30 N standard deviation claimed in [19]. Nonetheless, we believe our results are a more accurate reflection of the precision possible in the system.

4) Goodness of Fit: Both the surface fit and the linear fit are sufficient for the main purpose of the tool: securing tissue without damaging it. Using 160 kPA as the upper limit on pressure at the jaw tips as suggested in [5] limits the maximum applied force to 9 newtons. Heijnsdijk *et al.* found the minimum force to securely grasp tissue to be approximately 3 N for surgical graspers with similar profiles [4]. These bounds leave a 6 N effective operating range, and large enough window even with a standard deviation of approximately 1 N. If future work requires more precise force measurements then either the calibration process needs to be refined or a better method of force sensing needs to be implemented.

Moreover, the the near identical standard deviation of the surface fit that includes the encoder readings (0.980 N) and the curve fit that ignores the encoder readings (0.989 N) indicates that the jaw distance plays at a negligible role in determining the force applied at the Grasper's tip.

B. Position Calibration

1) Position Surface Fit: The best fit planar surface (Fig. 10) to the data gathered in section II-C is defined by:

$$d(x, y) = k_0 + k_1 x + k_2 y \qquad (6)$$

where x is the internal force sensor reading in DV, y is the encoder reading in counts, and d is jaw distance in millimeters. Values for the k_0, k_1, and k_2 coefficients can be found in Table IV. The fit has an RSME of 0.742 mm and a MAE of 0.575 mm.

TABLE IV: Position Coefficient Values

Coefficient	Value	Unit
k_0	80.3	mm
k_1	1.88×10^{-2}	mm per Grasper DV
k_2	1.07×10^{-3}	mm per encoder count

The error between the measured and calculated position values for a given set of force and encoder readings (Fig. 10c) appears to be normally distributed around zero (the calculated mean error is -1.03×10^{-12} mm). This implies that (6) can be rewritten as:

$$d(x, y) = k_0 + k_1 x + k_2 y + \epsilon(\mu, \sigma) \qquad (7)$$

where ϵ is a Gaussian distribution with mean $\mu = 0$ and standard deviation $\sigma = 0.743$ mm. The formulation in (7) can then be propagated forward when evaluating sensor readings with position-dependent modalities such as ultrasound.

2) Comparison to Previous Work: Like [19], we use regression to determine an equation relating the measured force and encoder values to the jaw distance. Our measured standard deviation of 0.743 mm is larger than Roan's reported standard deviation of 0.2834 mm. Nonetheless, we believe our results are more robust for current state of the Grasper.

First, whereas we used a machined fixture to collect position data, while Roan *et al.* used cardboard "structures" to set the jaw distance for calibration [19, p. 181]. Accurately measuring the jaw distance without a proper calibration fixture is difficult, so there are likely meaningful measurement errors that are unaccounted for in the stated standard deviation.

Second [19] overfit the curve to their data. Roan *et al.*'s regression has eight terms [19] compared to just three terms in (6). While [19]'s surface may fit the collected data very well, it is less likely to fit other points in the space over which the grasper will operate.

IV. CONCLUSION AND FUTURE WORK

This work demonstrates the calibration setup and procedure for joint calibration of a motorized endoscope Smart Grasper using both force and encoder outputs. While our results may have greater uncertainty as previous calibration work, our more robust methodology means that the resulting calibration equations are a better reflection of the underlying system and are therefore more useful going forward.
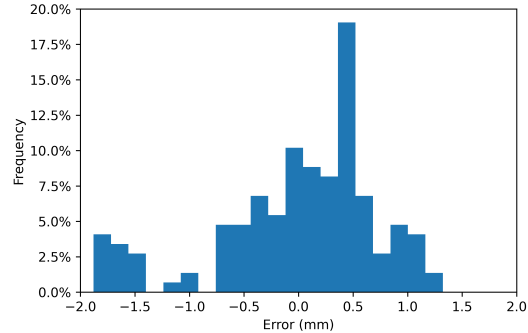
The next steps involve integrating the force and position readings into the device architecture that includes other sensors (pulse oximetry, bioimpedance, temperature, ultrasound)
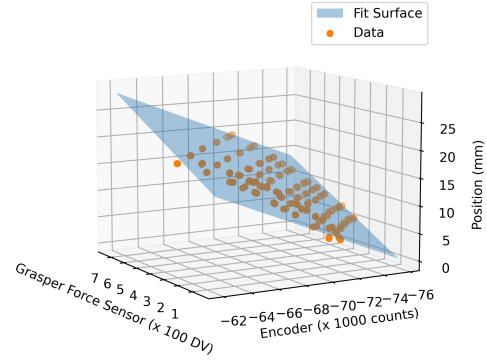
(a) Position surface fit plot
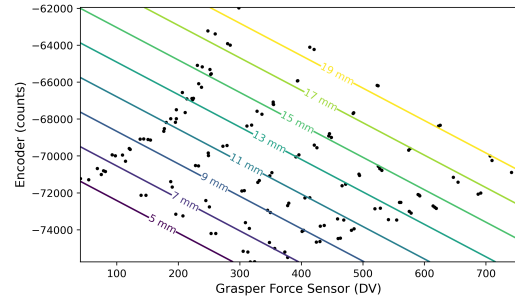
(b) Position fit contour plot

(c) Position fit error distribution

Fig. 10: Planar surface fit for position calibration. The best fit surface is plotted alongside (a) the measured data in 3D and (b) a 2D contour plot. The distribution of the error between the measured and calculated jaw distance for a given force-encoder pair is shown in (c).

and that will constitute the complete Smart Grasper. A force controller must then be implemented to ensure that the applied force at the Grasper tip stays within safe operation limits. Once integrated, we will collect multi-modal data from butcher meat. A machine learning algorithm will then process the data, fusing the various sensor information into an accurate tissue characterization.

REFERENCES

[1] T. D. Nagy and T. Haidegger, "Recent advances in robot-assisted surgery: Soft tissue contact identification," in *Proc. SACI*, Timisoara, Romania, May 29–31, 2019, pp. 99–106.

[2] S. Schostek, M. O. Schurr, and G. F. Buess, "Review on aspects of artificial tactile feedback in laparoscopic surgery," *Med. Eng. Phys.*, vol. 31, no. 8, pp. 887–898, Oct. 2009.

[3] J. Konstantinova, A. Jiang, K. Althoefer, P. Dasgupta, and T. Nanayakkara, "Implementation of tactile sensing for palpation in robot-assisted minimally invasive surgery: A review," *IEEE Sens. J.*, vol. 14, no. 8, pp. 2490–2501, Aug. 2014.

[4] E. A. M. Heijnsdijk, H. de Visser, J. Dankelman, and D. J. Gouma, "Slip and damage properties of jaws of laparoscopic graspers," *Surg. Endosc.*, vol. 18, no. 6, pp. 974–979, Jun. 2004.

[5] J. Rosen, J. D. Brown, S. De, M. Sinanan, and B. Hannaford, "Biomechanical properties of abdominal organs in vivo and postmortem under compression loads," *J. Biomech. Eng.*, vol. 130, no. 2, Apr. 2008, Art. no. 021020.

[6] D.-H. Lee, U. Kim, T. Gulrez, W. J. Yoon, B. Hannaford, and H. R. Choi, "A laparoscopic grasping tool with force sensing capability," *IEEE/ASME Trans. Mech.*, vol. 21, no. 1, pp. 130–141, Feb. 2016.

[7] B. Hannaford, J. Rosen, D. W. Friedman, H. King, P. Roan, L. Cheng, D. Glozman, J. Ma, S. N. Kosari, and L. White, "Raven-II: An open platform for surgical robotics research," *IEEE Trans. Biomed. Eng.*, vol. 60, no. 4, pp. 954–959, Apr. 2013.

[8] U. Kim, D.-H. Lee, W. J. Yoon, B. Hannaford, and H. R. Choi, "Force sensor integrated surgical forceps for minimally invasive robotic surgery," *IEEE Trans. Robot.*, vol. 31, no. 5, pp. 1214–1224, Oct. 2015.

[9] U. Kim, Y. B. Kim, D.-Y. Seok, J. So, and H. R. Choi, "Development of surgical forceps integrated with a multi-axial force sensor for minimally invasive robotic surgery," in *Proc. IROS*, Daejeon, Korea (South), Oct. 9–14, 2016, pp. 3684–3689.

[10] D.-Y. Seok, Y. B. Kim, U. Kim, S. Y. Lee, and H. R. Choi, "Compensation of environmental influences on sensorized-forceps for practical surgical tasks," *IEEE Robot. Automat. Lett.*, vol. 4, no. 2, pp. 2031–2037, Apr. 2019.

[11] G. S. Fischer, T. Akinbiyi, S. Saha, J. Zand, M. Talamini, M. Marohn, and R. Taylor, "Ischemia and force sensing surgical instruments for augmenting available surgeon information," in *Proc. BioRob*, Pisa, Italy, Feb. 20-22, 2006, pp. 1030–1035.

[12] G. Tholey and J. P. Desai, "A modular, automated laparoscopic grasper with three-dimensional force measurement capability," in *Proc. ICRA*, Rome, Italy, Apr. 10–14, 2007, pp. 250–255.

[13] S. Sokhanvar, M. Packirisamy, and J. Dargahi, "MEMS endoscopic tactile sensor: Toward in-situ and in-vivo tissue softness characterization," *IEEE Sens. J.*, vol. 9, no. 12, pp. 1679–1687, Dec. 2009.

[14] K. Sun, M. Li, S. Wang, G. Zhang, H. Liu, and C. Shi, "Development of a fiber Bragg grating-enabled clamping force sensor integrated on a grasper for laparoscopic surgery," *IEEE Sens. J.*, May 2021, (Early Access).

[15] L. Li, B. Yu, C. Yang, P. Vagdargi, R. A. Srivatsan, and H. Choset, "Development of an inexpensive tri-axial force sensor for minimally invasive surgery," in *2017 IEEE/RSJ International Conference on Intelligent Robots and Systems (IROS)*, Vancouver, BC, Canada, Sep. 24–28 2017, pp. 906–913.

[16] T. G. Frank, G. B. Hanna, and A. Cuschieri, "Technological aspects of minimal access surgery," *Proc. Inst. Mech. Eng. H*, vol. 211, no. 2, pp. 129–144, Feb. 1997.

[17] U. Kim, Y. B. Kim, J. So, D.-Y. Seok, and H. R. Choi, "Sensorized surgical forceps for robotic-assisted minimally invasive surgery," *IEEE Trans. Ind. Electron.*, vol. 65, no. 12, pp. 9604–9613, Dec. 2018.

[18] J. D. Brown, J. Rosen, M. Moreyra, M. Sinanan, and B. Hannaford, "Computer-controlled motorized endoscopic grasper for in vivo measurement of soft tissue biomechanical characteristics," in *Proc. MMVR 02/10*, ser. Studies in Health Technology and Informatics, vol. 85, 2002, pp. 71–73.

[19] P. R. Roan, A. S. Wright, T. S. Lendvay, M. N. Sinanan, and B. Hannaford, "An instrumented minimally invasive surgical tool: Design and calibration," *Appl. Bionics Biomech.*, vol. 8, no. 2, pp. 173–190, 2011.

[20] P. R. Roan, "An instrumented surgical tool for local ischemia detection," Ph.D. Dissertation, Dept. Elect. Eng., Univ. Washington, Seattle, WA, USA, Apr. 2011.